FACTA UNIVERSITATIS
Series: **Physics, Chemistry and Technology** Vol. 22, Nº 1, 2024, pp. 25 - 36
https://doi.org/10.2298/FUPCT2401025D

Original scientific paper

DIFFERENTIAL CROSS SECTIONS FOR ELECTRON CAPTURE FROM ATOMIC HYDROGEN BY FAST ALPHA PARTICLES

Danilo Delibašić, Nenad Milojević, Ivan Mančev

Department of Physics, Faculty of Sciences and Mathematics, University of Niš, Niš, Serbia

ORCID iDs: Danilo Delibašić https://orcid.org/0000-0003-3094-4304
Nenad Milojević https://orcid.org/0000-0002-5639-2192
Ivan Mančev https://orcid.org/0000-0002-8955-1938

Abstract. *Electron capture in collisions of fast alpha particles with atomic hydrogen is studied by means of the prior version of the three-body boundary-corrected intermediate-states method (BCIS-3B). State-selective and state-summed differential cross sections are presented for the final state n up to $n_{\max} = \{2,3,4\}$, depending on the incident energy. The contributions from higher excited states with $n > n_{\max}$ are included using the Oppenheimer n^{-3} scaling law. The observed angular dependencies of the obtained differential cross sections are analyzed in detail, for incident projectile energy values of $E = \{100,\ 150,\ 300\}\ \frac{\text{keV}}{\text{amu}}$ (intermediate) and $E = \{1.3,\ 2.5,\ 5.0,\ 7.5,\ 12.5\}\ \frac{\text{MeV}}{\text{amu}}$ (high energy values).*

Key words: *ion-atom collisions, electron capture, differential cross sections*

1. INTRODUCTION

Electron capture in ion-atom collisions is a physical process that has attracted a lot of attention, both from theoretical and experimental perspectives. The interest in studying electron capture is two-fold. From a purely fundamental standpoint, there is a clear incentive to understand the underlying mechanisms of electron capture, in the context of quantum theory. From an application-oriented standpoint, electron capture cross sections are of crucial importance in interdisciplinary areas, which include plasma physics, thermonuclear fusion research, astrophysics and medical physics (hadron radiotherapy). Cross section values are needed for the evaluation of electron capture overall energy balance, which is crucial in plasma diagnostics and thermonuclear fusion (Anderson et al., 2000; Donné et al., 2007; Hemsworth et al., 2009; Isler, 1994; Marchuk, 2014; Ralchenko et al., 2008; Thomas, 2012), as well as astrophysics (Cravens, 2002; Heng and Sunyaev,

Received: December 17th, 2024; accepted: December 24th, 2024
Corresponding author: Danilo Delibašić
Department of Physics, Faculty of Sciences and Mathematics, University of Niš, Višegradska 33, 18000 Niš, Serbia
E-mail: danilo.delibasic@pmf.edu.rs

2008). In hadron radiotherapy, dose planning systems must include the contributions from energy losses due to charge exchange (Alberg-Fløjborg, 2020; Belkić, 2010; Belkić, 2021a; Belkić, 2021b; Ebner and Kamada, 2016; Rivarola, 2013; Suit, 2010), which are given in the form of cross section values (either calculated or measured).

A purely three-body problem, where the projectile is a completely stripped ion, while the target is a hydrogen-like atom/ion, is the simplest system where electron capture can be studied. Three-body problems can therefore be used as a benchmark testing ground for theoretical approaches to treating single-electron capture. The topic of the present work is exactly one such process, of electron capture in collision between fast alpha particles and hydrogen atoms in their ground states. Usually, findings on the values of differential and total cross sections are reported. Of the two, a more stringent test of the theory is its performance regarding the differential cross sections, which usually exhibit much more nuance than total cross sections. This is precisely the reason why this work reports on the differential cross sections, in the framework of the three-body boundary-corrected intermediate-states method (BCIS-3B). This method was first developed for ground-to-arbitrary state capture recently in Milojević et al., 2020, and further applied to a wide array of processes in Delibašić et al., 2021a; Delibašić et al., 2021b and Delibašić et al., 2022. This work presents the first application of the BCIS-3B method to calculate the differential cross sections in $\alpha + \mathrm{H}(1\mathrm{s})$ collisions, for ground-to-arbitrary state capture.

The prior form BCIS-3B method admits the same perturbation potential and asymptotic wavefunction in the entrance channel as the prior form CB1-3B, i.e. the three-body boundary-corrected first-Born approximation (Belkić et al., 1979). In the exit channel, the asymptotic wavefunction is the same as in the three-body continuum distorted-wave method (CDW-3B) from Belkić et al., 1979 and Cheshire, 1964. While CB1-3B is a first-order theory, the presence of the continuum wave makes BCIS-3B a second-order theory. This enables the BCIS-3B method to predict Thomas double scattering, which is distinctly a second-order effect, and as such cannot be predicted by first-order theories. Due to the use of eikonal hypothesis, the BCIS-3B method is a high-energy theory. Thus, it is expected to produce valid results predominantly in the high-energy region ($E > 400\ \frac{\mathrm{keV}}{\mathrm{amu}}$), as well as possibly in the intermediate energy region ($E \in [25,\ 400]\ \frac{\mathrm{keV}}{\mathrm{amu}}$), although to a lesser extent.

There are unfortunately no available experimental data on the differential cross section values for $\alpha + \mathrm{H}(1\mathrm{s})$ collisions. However, due to the previously demonstrated success of the BCIS-3B method in comparison with available measurements for differential cross sections in $p + \mathrm{H}(1\mathrm{s})$ collisions (Milojević et al., 2020), as well as total cross sections in various other processes (Milojević et al., 2020; Delibašić et al., 2021a; Delibašić et al., 2021b; Delibašić et al., 2022), the presently reported cross sections can be taken as a trustworthy theoretical benchmark. Possible future measurements would thus greatly benefit from a comparison with hereby given differential cross section values. The differential cross sections for electron capture in $\alpha + \mathrm{H}(1\mathrm{s})$ collisions obtained via theoretical coupled-state calculations were previously reported in Winter et al., 1987 and Winter, 1988, but only for the low to low-intermediate energy region. The process of electron capture in $\alpha + \mathrm{H}(1\mathrm{s})$ collisions was also recently studied via the standard three-body classical trajectory Monte Carlo (CTMC) and quasi-classical trajectory Monte Carlo (QCTMC) models in Ziaeian and Tőkési, 2022 (only total cross sections were reported).

Atomic units will be used throughout unless otherwise stated.

2. THEORY

The process of electron capture in $\alpha + \mathrm{H}(1s)$ collisions is analyzed in the wider framework of collisions between fast completely stripped projectiles and hydrogen-like targets in their ground states, for various levels of state-resolved final states:

$$Z_\mathrm{P} + (Z_\mathrm{T}, e)_{1s} \rightarrow (Z_\mathrm{P}, e)_{nlm} + Z_\mathrm{T}, \tag{1}$$

$$Z_\mathrm{P} + (Z_\mathrm{T}, e)_{1s} \rightarrow (Z_\mathrm{P}, e)_{nl} + Z_\mathrm{T}, \tag{2}$$

$$Z_\mathrm{P} + (Z_\mathrm{T}, e)_{1s} \rightarrow (Z_\mathrm{P}, e)_{n} + Z_\mathrm{T}, \tag{3}$$

$$Z_\mathrm{P} + (Z_\mathrm{T}, e)_{1s} \rightarrow (Z_\mathrm{P}, e)_{\Sigma} + Z_T. \tag{4}$$

In Eqs. (1)-(4), Z_P and Z_T represent the charges of the projectile P and target nucleus T, with masses M_P and M_T, respectively, and e represents the electron. All Eqs. (1)-(4) pertain to electron capture which occurs from the ground state 1s of the hydrogen-like target, into an arbitrary nlm final state of the projectile, with the $\{n, l, m\}$ being the usual triplet of quantum numbers. Eqs. (1), (2) and (3) represent capture from the ground state into arbitrary final states nlm, arbitrary subshells nl and shells n, respectively. Eq. (4) represents electron capture into arbitrary (all) the final states of the projectile.

The transition amplitude matrix elements in the prior form of the BCIS-3B method are given by (Milojević et al., 2020):

$$T_{nlm,100}(\vec{\eta}) = N^+(\nu_\mathrm{T})\, Z_\mathrm{P} \int\int d\vec{s} d\vec{R}\, \varphi^*_{nlm}(\vec{s}) \left(\frac{1}{R} - \frac{1}{s}\right) \varphi_{100}(\vec{x}) e^{i\vec{\beta}\cdot\vec{R} - i\vec{v}\cdot\vec{s}}$$

$$\times F(i\nu_\mathrm{T}, 1, ivx + i\vec{v}\cdot\vec{x}) \left(vR + \vec{v}\cdot\vec{R}\right)^{i\xi}, \tag{5}$$

with the following nomenclature: $\xi = Z_\mathrm{P}/v$, $\nu_\mathrm{T} = Z_\mathrm{T}/v$ and $N^+(\nu_\mathrm{T}) = \Gamma(1 - i\nu_\mathrm{T}) e^{\pi\nu_\mathrm{T}/2}$. The projectile velocity along the z-axis is denoted by $\vec{v}$, the momentum transfer by $\vec{\beta} = -\vec{\eta} + \beta_z \hat{\vec{v}}$, and its component along the $z-$ axis by $\beta_z = -v/2 - \Delta E/v$. The difference between the initial and final bound state energies is given by $\Delta E = E_1^H - E_1^{He}$. The transverse momentum transfer vector is given by $\vec{\eta} = (\eta\, cos\, \phi_\eta\, , \eta\, sin\, \phi_\eta\, , 0)$, and satisfies the property $\vec{\eta}\cdot\vec{v} = 0$. Vectors $\vec{x}$ and $\vec{s}$ represent the position vectors of the electron relative to the target and projectile, respectively, and $\vec{R}$ is the relative position vector of the projectile to the target. The bound-state wavefunctions of the initial, ground-state hydrogen-like target $(Z_\mathrm{T}, e)_{1s}$, and the final, arbitrary-state hydrogen-like projectile system $(Z_\mathrm{P}, e)_{nlm}$, are denoted by $\varphi_{100}(\vec{x})$ and $\varphi_{nlm}(\vec{s})$, respectively. Lastly, $F(i\nu_\mathrm{T}, 1, ivx + i\vec{v}\cdot\vec{x})$ represents the confluent hypergeometric function.

The amplitude matrix elements given by Eq. (5) are in the form of six-dimensional integrals. Fortunately, some of the integrations can be performed analytically (Milojević et al., 2020), allowing T_{if} to be reduced to a two-dimensional integral over real variables in the interval [0,1]. The state-selective differential cross sections for capture into an arbitrary final state nlm of the projectile are then given by:

$$\frac{dQ_{nlm}}{d\Omega}\left(\frac{a_0^2}{\mathrm{sr}}\right) = \frac{\mu^2}{4\pi^2} |\mathrm{T_{if}}(\vec{\eta})|^2, \tag{6}$$

where $\mu = \frac{M_\mathrm{P} M_\mathrm{T}}{M_\mathrm{P} + M_\mathrm{T}}$ is the reduced mass of the collisional system. The state-selective differential cross sections for capture into nl subshells and n shells are then, respectively, given by:

$$\frac{dQ_{nl}}{d\Omega} = \sum_{m=-l}^{+l} \frac{dQ_{nlm}}{d\Omega}, \quad \frac{dQ_n}{d\Omega} = \sum_{l=0}^{n-1} \frac{dQ_{nl}}{d\Omega}. \tag{7}$$

The final step would be the calculation of the state-summed differential cross sections, taking into account the contributions from all possible n. Since this is clearly not possible, cross sections $\frac{dQ_n}{d\Omega}$ were calculated up to some value $n_{\max}$, while the contributions to the state-summed total cross sections from higher excited final states with $n > n_{\max}$ were included via the Oppenheimer n^{-3} scaling law (Oppenheimer, 1928). The choice of $n_{\max}$ was energy dependent, since the contribution from higher excited states becomes negligible with increasing incident energy values. Due to this fact, we set $n_{\max} = 4$ for $E = \{100, 150, 300, 1300\} \frac{\text{keV}}{\text{amu}}$, $n_{\max} = 3$ for $E = \{2.5, 5.0\} \frac{\text{MeV}}{\text{amu}}$, and $n_{\max} = 2$ for $E = \{7.5, 12.5\} \frac{\text{MeV}}{\text{amu}}$. All these choices for $n_{\max}$ were sufficient, as will be shown in the Results and discussion section. The Oppenheimer n^{-3} scaling law, applied for $n_{\max} = \{2, 3, 4\}$, results in the following expressions for state-summed differential cross sections:

$$\frac{dQ}{d\Omega} = \frac{dQ_1}{d\Omega} + \frac{dQ_2}{d\Omega} + \frac{dQ_3}{d\Omega} + 2.561 \frac{dQ_4}{d\Omega}, \tag{8}$$

$$\frac{dQ}{d\Omega} = \frac{dQ_1}{d\Omega} + \frac{dQ_2}{d\Omega} + 2.081 \frac{dQ_3}{d\Omega}, \tag{9}$$

$$\frac{dQ}{d\Omega} = \frac{dQ_1}{d\Omega} + 1.616 \frac{dQ_2}{d\Omega}, \tag{10}$$

with $\frac{dQ}{d\Omega} \equiv \frac{dQ_\Sigma}{d\Omega}$.

Numerical integrations in Eq. (5) were performed via the Gauss-Legendre quadrature rules. The condition of convergence to at least two decimal places for both the state-selective and state-summed differential cross sections was imposed, for every energy value considered. The same number of integration points was used per each of the two integration axes. Convergence becomes a more prominent issue with increasing energy values, as well as increasing n values. For the lowest examined energy values, a total of 368 integration points were sufficient along each of the two integration axes, while up to 2256 integration points were needed for $E = 12.5 \frac{\text{MeV}}{\text{amu}}$ and $n = 2$.

3. Results and Discussion

Differential cross sections, both state-selective and state-summed, were calculated in the intermediate and high energy range for electron capture in the following collisional process:

$$\alpha + \text{H}(1\text{s}) \rightarrow \text{He}^+(\Sigma) + p, \tag{11}$$

where α represents an alpha particle (completely stripped helium He^{2+}), and p represents a proton. The results were graphically represented in Figures 1-8. Unfortunately, there are no available experimental data to make a comparison with, and truly assess the validity of the present theoretical method. However, the BCIS-3B method was previously demonstrated to be in great agreement with measurements, for a very wide variety of projectiles and targets, as well as incident energy values, regarding both differential and total cross sections (Milojević et al., 2020; Delibašić et al., 2021a; Delibašić et al., 2021b; Delibašić et al., 2022). Thus, the differential cross sections presented in this work can be taken with a high level of confidence

and could be used as benchmarks for other theoretical methods (as well as experimental results). Of course, possible future measurements would be highly desirable, to compare with the present theoretical findings.

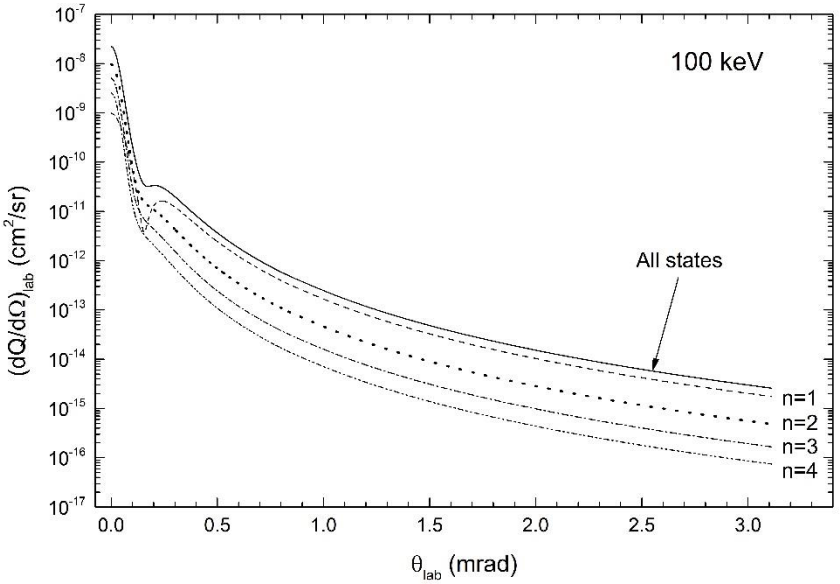

Fig. 1 State-selective and state-summed differential cross sections $\left(\frac{dQ_{\Sigma}}{d\Omega}\right)_{lab} \equiv \left(\frac{dQ}{d\Omega}\right)_{lab} \left(\frac{\mathrm{cm}^2}{\mathrm{sr}}\right)$ for process $\boldsymbol{\alpha + \mathrm{H}(1s) \rightarrow \mathrm{He}^{+} + p}$ as a function of scattering angle $\boldsymbol{\theta_{lab}}$ in the laboratory frame, for incident energy $\boldsymbol{E = 100 \frac{\mathrm{keV}}{\mathrm{amu}}}$. All the results are from the present theoretical BCIS-3B method: dashed line – capture into $\boldsymbol{n = 1}$ final state, dotted line – capture into $\boldsymbol{n = 2}$ final state, dashed-dotted line – capture into $\boldsymbol{n = 3}$ final state, dashed-double-dotted line – capture into $\boldsymbol{n = 4}$ final state, full line – capture into any final state.

Figs. 1-3 show the present theoretical results for state-selective and state-summed differential cross sections in $\alpha + \mathrm{H}(1s)$ collisions for intermediate incident projectile energy values $E = \{100,\ 150,\ 300\} \frac{\mathrm{keV}}{\mathrm{amu}}$, respectively. All these results explicitly include state-selective cross sections values for capture up to $n_{\max} = 4$. All three Figs. 1-3 show that the cross sections attain their maximal value for forward scattering, i.e. at $\theta = 0$ mrad, followed by a sharp drop. A change of slope of the curves can be seen at about $\theta = 0.15 - 0.2$ mrad, followed by a long tail. This holds for all the state-selective cross sections, as well as state-summed. These profiles are a consequence of two competing mechanisms: electronic and nuclear motions. The electron-nucleus interaction dominates at smaller angles, which manifests as the forward peak. The nucleus-nucleus elastic Rutherford scattering has negligible effects in the vicinity of the forward cone but becomes the dominant scattering mechanism at larger angles, exhibiting a long tail. The interference of these competing effects results in the observed cross section profiles.

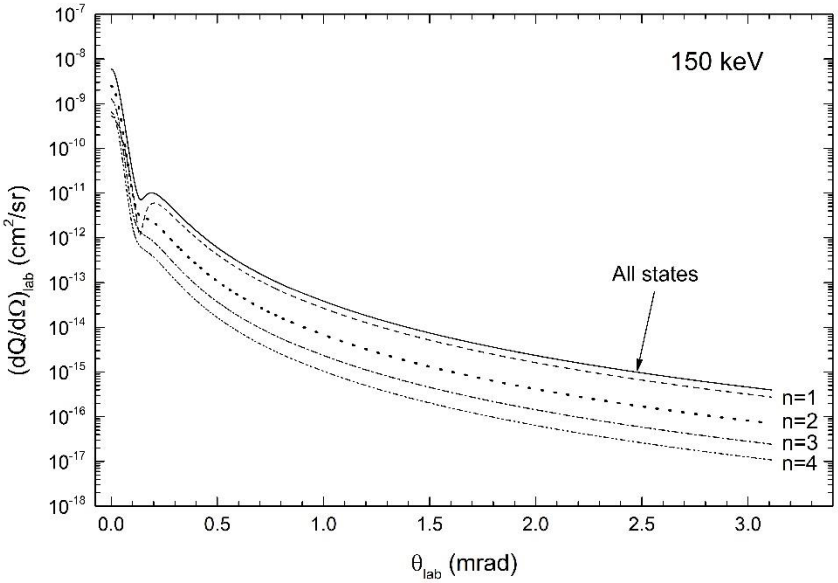

Fig. 2 The same as in Fig. 1, except for incident energy $\boldsymbol{E = 150\,\frac{keV}{amu}}$.

In all three Figs. 1-3, for larger angles (Rutherford scattering) the cross sections $\frac{dQ_1}{d\Omega}$ dominate, with the contribution from each higher $\frac{dQ_n}{d\Omega}$, $n > 1$ being significantly lesser than the previous one. The forward scattering case exhibits a different pattern, however. In Fig. 1, the $\frac{dQ_2}{d\Omega}$ contribution dominates, followed by $\frac{dQ_3}{d\Omega}$ and $\frac{dQ_4}{d\Omega}$, while $\frac{dQ_1}{d\Omega}$ provides the least significant contribution. The situation slowly shifts with rising energy, however, as Fig. 2 displays the contribution from $\frac{dQ_1}{d\Omega}$ to be on par with the one from $\frac{dQ_4}{d\Omega}$, while in Fig. 3 it holds that $\frac{dQ_2}{d\Omega} > \frac{dQ_1}{d\Omega} > \frac{dQ_3}{d\Omega} > \frac{dQ_4}{d\Omega}$.

Differential cross section profiles shown in Fig. 1 and Fig. 2 exhibit a minimum at about $\theta \approx 0.1$ mrad (the so-called *dark angle*), which can be seen in $\frac{dQ_1}{d\Omega}$ and $\frac{dQ_\Sigma}{d\Omega}$. These dips are most likely unphysical and would not be reproduced in measurements (as in the $p + \mathrm{H}(1s)$ collisions case, seen in Milojević et al., 2020). The dip results from the mutual cancellation of the perturbation potential nucleus-nucleus and nucleus-electron terms, i.e. $\frac{Z_P}{R} - \frac{Z_P}{s}$. The dip is entirely masked for $\frac{dQ_n}{d\Omega}$, $n \in \{2, 3, 4\}$. by the constructive interference terms of highly oscillatory behavior of the electronic full Coulomb wave function in the transition matrix integrand. Fig. 3 displays such minima for all $\frac{dQ_n}{d\Omega}$, $n \in \{1, 2, 3, 4\}$. The position of the dark angle shifts to lower values with increasing incident energy, as can be seen in Figs. 1-3.

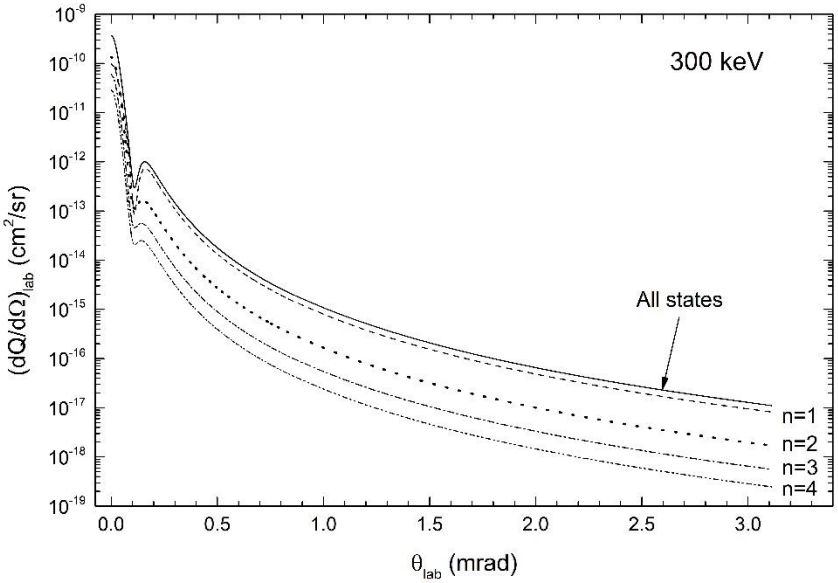

Fig. 3 The same as in Fig. 1, except for incident energy $\boldsymbol{E = 300\,\frac{keV}{amu}}$.

Figs. 4-8 show the present theoretical results for state-selective and state-summed differential cross sections in $\alpha + H(1s)$ collisions for high incident projectile energy values $\boldsymbol{E} = \{\boldsymbol{1.3}, \boldsymbol{2.5}, \boldsymbol{5.0}, \boldsymbol{7.5}, \boldsymbol{12.5}\}\,\frac{\boldsymbol{MeV}}{\boldsymbol{amu}}$, respectively. Fig. 4 for $\boldsymbol{E = 1.3}\,\frac{MeV}{amu}$ explicitly includes the contributions from capture up to $\boldsymbol{n}_{max} = \boldsymbol{4}$. Due to the already negligible contributions from $\frac{\boldsymbol{dQ_4}}{\boldsymbol{d\Omega}}$ at $\boldsymbol{E = 1.3}\,\frac{MeV}{amu}$, explicit contributions up to $\boldsymbol{n}_{max} = \boldsymbol{3}$ were included at $\boldsymbol{E = 2.5}\,\frac{MeV}{amu}$ and $\boldsymbol{E} = \boldsymbol{5}\,\frac{MeV}{amu}$ in Fig. 5 and Fig. 6, respectively. Due to the already negligible contributions from $\frac{\boldsymbol{dQ_3}}{\boldsymbol{d\Omega}}$ at $\boldsymbol{E = 5}\,\frac{MeV}{amu}$, explicit contributions up to $\boldsymbol{n}_{max} = \boldsymbol{2}$ were included at $\boldsymbol{E = 7.5}\,\frac{MeV}{amu}$ and $\boldsymbol{E} = \boldsymbol{12.5}\,\frac{MeV}{amu}$ in Fig. 7 and Fig. 8, respectively.

As can be seen in all the Figs. 4-8, all the state-selective and state-summed differential cross sections follow the same angular profile (qualitatively), with $\frac{\boldsymbol{dQ_n}}{\boldsymbol{d\Omega}} < \frac{\boldsymbol{dQ_{n-1}}}{\boldsymbol{d\Omega}}$, for all the displayed $\boldsymbol{n}$. This holds for all the five high energy values considered. An obvious feature in all these profiles is a second peak, in addition to the forward scattering one. This peak corresponds to the Thomas double scattering of the captured electron, which the BCIS-3B method correctly predicts, as a second-order theory. This effect is the quantum mechanical counterpart of the classical Thomas two-step billiard-type collision, where the electron first collides with the projectile, then the target, and finally being captured by the projectile.

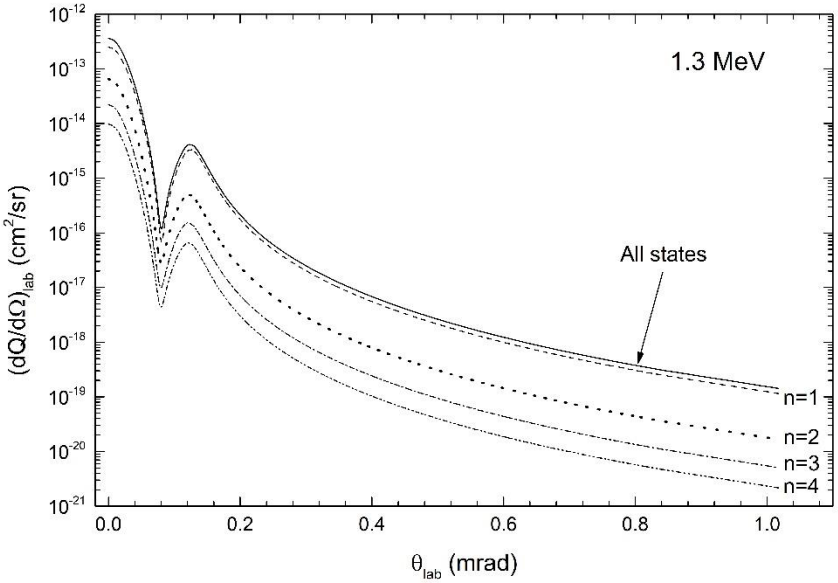

Fig. 4 The same as in Fig. 1, except for incident energy $\boldsymbol{E = 1.3\,\frac{MeV}{amu}}$.

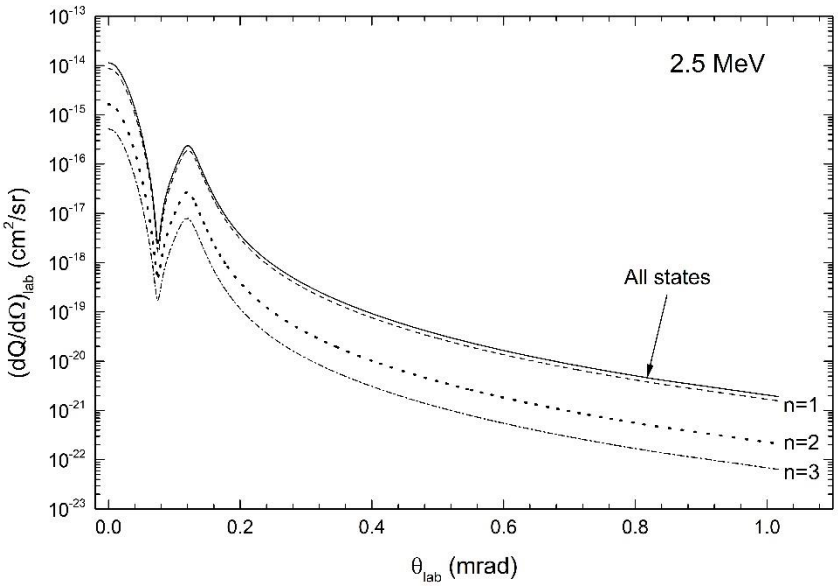

Fig. 5 The same as in Fig. 1, except for incident energy $\boldsymbol{E = 2.5\,\frac{MeV}{amu}}$ and capture up to $\boldsymbol{n = 3}$.

The projectile is (in the classical picture) deflected at the angle $\theta_{ds} = \frac{1}{M_P}\frac{\sqrt{3}}{2}$, which is located at $\theta_{ds} \approx 0.12\,mrad$ (lab) in the case of an alpha particle projectile. As can be seen in Figs. 4-8, in the quantum mechanical picture, a peak in differential cross sections is predicted at about this angle value. This is a feature predicted in all the second order theories and is experimentally observed (e.g. for $p + \mathrm{H}(1s)$ collisions in Vogt et al., 1986). Forward scattering dominates with respect to the Thomas double scattering peak for all the displayed incident energies. However, the relative magnitude of the Thomas double scattering peak, with respect to the forward scattering peak, increases with rising incident energy values. For energies even greater than $E = 12.5\,\frac{\mathrm{MeV}}{\mathrm{amu}}$, Thomas double scattering would eventually begin to dominate (not shown).

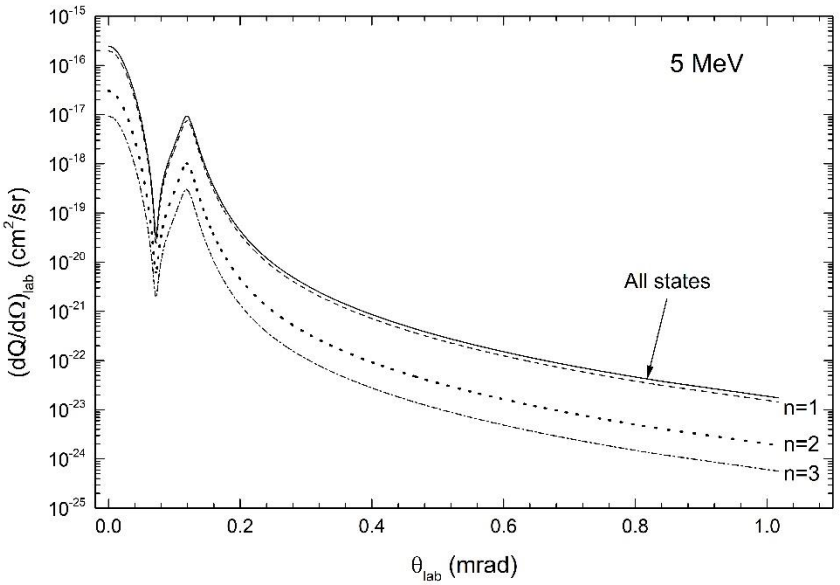

Fig. 6 The same as in Fig. 1, except for incident energy $\boldsymbol{E = 5\,\frac{\mathrm{MeV}}{\mathrm{amu}}}$ and capture up to $\boldsymbol{n = 3}$.

Between the forward and the Thomas double scattering peak, a minimum can be observed. This minimum in Figs. 4-8 for high incident energy values is, however, of a different nature than the one observed in Figs. 1-3 for intermediate incident energy values. This minimum stems from the destructive interference from the first- and second-order collisional events (Milojević et al., 2020), with each of them producing its own peak (forward and Thomas double scattering, respectively). For angles larger than θ_{ds}, Rutherford scattering dominates, which manifest as a long tail in the differential cross sections profile.

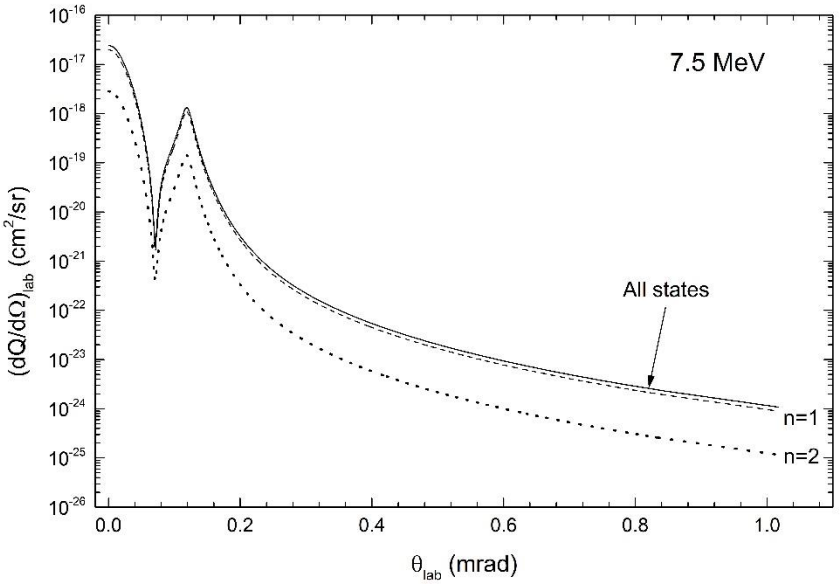

Fig. 7 The same as in Fig. 1, except for incident energy $\boldsymbol{E = 7.5\,\frac{MeV}{amu}}$ and capture up to $\boldsymbol{n = 2}$.

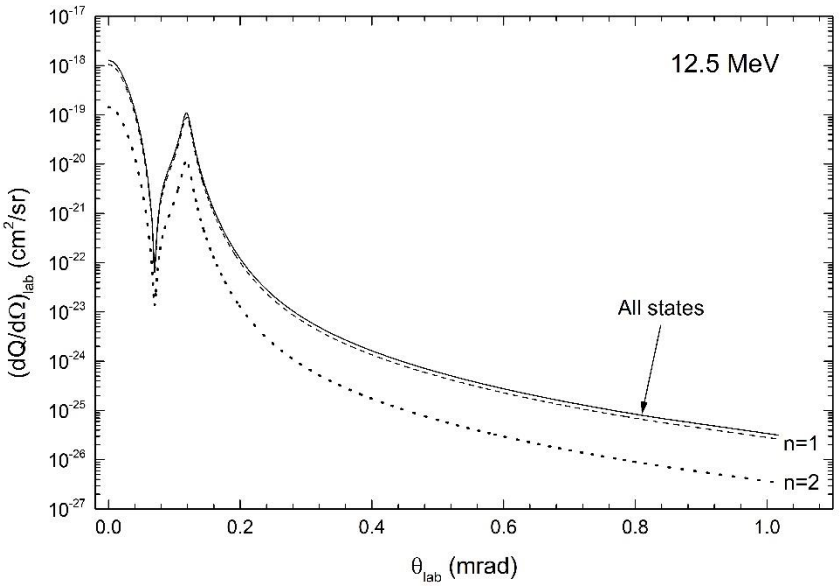

Fig. 8 The same as in Fig. 1, except for incident energy $\boldsymbol{E = 12.5\,\frac{MeV}{amu}}$ and capture up to $\boldsymbol{n = 2}$.

4. CONCLUSION

This work investigated electron capture in collisions between fast alpha particles and atomic hydrogen, using the BCIS-3B method (theoretical approach). State-selective and state-summed differential cross sections were calculated for incident projectile energy values belonging to the intermediate-energy range, for $E = \{100,\ 150,\ 300\}\ \frac{\text{keV}}{\text{amu}}$, as well as the high-energy range, for $E = \{1.3,\ 2.5,\ 5.0,\ 7.5,\ 12.5\}\ \frac{\text{MeV}}{\text{amu}}$. The explicit contributions from capture up to $n_{\max} = \{2,\ 3,\ 4\}$, with arbitrary lm, were included. The choice of $n_{\max}$ value depended on the incident projectile energy. When calculating the state-summed cross sections, contributions from higher excited states with $n > n_{\max}$ were approximated via the Oppenheimer n^{-3} scaling law. The obtained structures of the differential cross section profiles were analyzed in detail and their nature thoroughly explained. The BCIS-3B method, being a second-order theory, correctly predicts the Thomas double scattering mechanism, which is a prominent feature of high-energy ion-atom collisions.

Unfortunately, there are no available measurements for making a comparison with the presently obtained theoretical data. Nevertheless, the previously demonstrated success of the BCIS-3B method, in comparison with available experimental data for a great number of other electron capture processes, practically gives it a benchmark status. The obtained theoretical results could effectively be used for validation of the possible future measurements made for this electron capture process, especially for high-energy collisions.

Acknowledgement. *This research was supported by the Science Fund of the Republic of Serbia, Grant No 6821, Project title - ATMOLCOL. This research was also supported by the Ministry of Education, Science and Technological Development of the Republic of Serbia under Contract No. 451-03-65/2024-03/200124.*

REFERENCES

Alberg-Fløjborg A., Salo A. B., Solov'yov I. A., 2020. J. Phys. B, 53, 145202. doi:10.1088/1361-6455/ab8c56
Anderson H., von Hellermann M. G., Hoekstra R., Horton L. D., Howman A. C., Konig R. W. T., Martin R., Olson R .E., Summers H. P., 2000. Plasma Phys. Control. Fusion 42, 781. doi:10.1088/0741-3335/42/7/304
Belkić, Dž., Gayet, R., Salin, A., 1979. Phys. Rep., 56, 279–369. doi:10.1016/0370-1573(79)90035-8
Belkić Dž., 2010. J. Math. Chem., 47, 1366. doi:10.1007/s10910-010-9662-x
Belkić Dž., 2021a. Z. Med. Phys., 31, 122. doi:10.1016/j.zemedi.2020.07.003
Belkić Dž., 2021b. Adv. Quantum Chem., 84, 267. doi:10.1016/bs.aiq.2021.03.001
Cheshire, I. M., 1964. Proc. Phys. Soc. 84, 89. doi:10.1088/0370-1328/84/1/313
Cravens T. E., 2002. Science, 296, 1042. doi:10.1126/science.1070001
Delibašić D., Milojević N., Mančev I., Belkić Dž., 2021a. At. Data Nucl. Data Tables, 139, 101417. doi:10.1016/j.adt.2021.101417
Delibašić D., Milojević N., Mančev I., 2021b. Facta Universitatis, Series: Physics, Chemistry and Technology, 18(2), 131. doi:10.2298/FUPCT2002129D
Delibašić D., Milojević N., Mančev I., Belkić Dž., 2022. At. Data Nucl. Data Tables, 148, 101530. doi:10.1016/j.adt.2022.101530
Donné A. J. H., Costley A. E., Barnsley R. et al., 2007. Nucl. Fusion, 47, S337. doi:10.1088/0029-5515/47/6/S07
Ebner D. K., Kamada T., 2016. Front. Oncol., 6, 140. doi: 10.3389/fonc.2016.00140
Hemsworth R., Decamps H., Graceffa J., Schunke B., Tanaka M., Dremel M., Tanga A., De Esch H. P. L., Geli F., Milnes J., Inoue T., Marcuzzi D., Sonato P., Zaccaria P., 2009. Nucl. Fusion, 49, 045006. doi:10.1088/0029-5515/49/4/045006
Heng K., Sunyaev R.A., 2008. Astron. & Astrophys., 481, 117. doi:10.1051/0004-6361:20078906
Isler R. C., 1994. Plasma Phys. Control. Fusion, 36, 171. doi:10.1088/0741-3335/36/2/001

Marchuk O., 2014. Phys. Scr., 89, 114010. doi:10.1088/0031-8949/89/11/114010
Milojević N., Mančev I., Delibašić D. and Belkić Dž., 2020. Phys. Rev. A, 102, 012816. doi:10.1103/PhysRevA.102.012816
Oppenheimer J. R., 1928. Phys. Rev., 31, 349. doi:10.1103/PhysRev.31.349
Ralchenko Y., Draganić I .N., Tan J .N., Gillaspy J. D., Pomeroy J. M., Reader J., Feldman U., Holland G. E., 2008. J. Phys. B, 41, 021003. doi:10.1088/0953-4075/41/2/021003
Rivarola R. D., Galassi M. E., Fainstein P. D., Champion C., 2013. in: Belkić Dž. (Volume Ed.), Sabin J. R., Braňdas E. (Series Eds.), Theory of Ion Collision Physics in Hadron Therapy, Academic Press, Oxford: Adv. Quantum Chem., Ch 9, 65, p. 231.
Suit H., DeLaney T., Goldberg S., Paganetti H., Clasie B., Gerweck L., Niemierko A., Hall E., Flanz J., Hallman J., Trofimov A., 2010. Radioth. Oncol., 95, 3. doi:10.1016/j.radonc.2010.01.015
Thomas D. M., 2012. Phys. Plasmas, 19, 056118. doi:10.1063/1.3699235
Vogt H., Schuch R., Justiniano R., Shulz M., Schwab W., 1986. Phys. Rev. Lett., 57, 2256. doi: 10.1103/PhysRevLett.57.2256
Winter T. G., Hatton G. J., Day A. R., Lane F., 1987. Phys. Rev. A, 36, 625. doi:10.1103/PhysRevA.36.625
Winter T. G., 1988. Phys. Rev. A, 38, 1612. doi:10.1103/PhysRevA.38.1612
Ziaeian I., Tőkési K., 2022. At. Data Nucl. Data Tables, 146, 101509. doi:10.1016/j.adt.2022.101509

DIFERENCIJALNI EFIKASNI PRESECI ZA ELEKTRONSKI ZAHVAT IZ ATOMSKOG VODONIKA ALFA ČESTICAMA

Elektronski zahvat u sudarima brzih alfa čestica sa atomom vodonika je izučavan u okviru prior verzije tročestičnog granično korektnog metoda sa kontinuumskim intermedijarnim stanjima (BCIS-3B). Parcijalni i sumirani diferencijalni efikasni preseci su predstavljeni za finalna stanja sa glavnim kvantnim brojem n do $n_{\max} = \{2,3,4\}$, u zavisnosti od vrednosti incidentne energije projektila. Efikasni preseci su izračunati za zahvat u proizvoljna finalna stanja projektila sa orbitalnim i magnetnim kvantnim brojevima lm. Doprinosi efIkasnim presecima od strane viših pobuđenih stanja $n > n_{\max}$ uračunati su korišćenjem Openhajmerovog n^{-3} zakona skaliranja. Dobijene ugaone zavisnosti diferencijalnih efikasnih preseka su detaljno analizirane, za vrednosti incidentne energije projektila $E = \{100,\ 150,\ 300\}\ \frac{\text{keV}}{\text{amu}}$ (srednje) i $E = \{1.3,\ 2.5,\ 5.0,\ 7.5,\ 12.5\}\ \frac{\text{keV}}{\text{amu}}$ (visoke vrednosti energije).

Ključne reči: *jon-atomski sudari, elektronski zahvat, diferencijalni efikasni preseci*